Proceedings of the 16th International Conference on Soil Mechanics and Geotechnical Engineering

doi:10.3233/978-1-61499-656-9-795

Physical and numerical modeling of cyclic moment-rotation behavior of shallow foundations

Modélisation physique et numérique du comportement cyclique de moment-rotation de fondations "superficielles"

Sivapalan Gajan, Bruce L Kutter & Jeremy M Thomas
University of California, Davis, USA

ABSTRACT

Six series of tests on a large centrifuge, including 50 models of shallow foundations supporting shear walls, were performed to study the nonlinear load-deformation characteristics of shallow foundations during cyclic and earthquake loading. Rocking of the footing during cyclic loading progressively rounds the foundation soil, and this rounding causes a reduction in contact area between the footing and soil thereby causing a nonlinearity and stiffness reduction on the moment-rotation relationship. Analytical modeling was carried out to model the moment-rotation behavior of footing-soil interface. The rigid footing and the soil beneath were modeled as a single element that captures the essential features of the moment-rotation behavior that were observed in the centrifuge experiments.

RÉSUMÉ

Afin d'étudier les caractéristiques non-linéaires charge-déplacement de fondations superficielles pour des charges cycliques ainsi que sismiques, six séries d'essai ont été effectuées sur une grande centrifugeuse, comprenant 50 modèles de fondations superficielles supportant des murs de cisaillement. Le basculement de la fondation sous la charge cyclique arrondit le sol de fondation progressivement, ce qui provoque une réduction de la surface de contact entre la fondation et le sol, engendrant une non-linéarité et une réduction de rigidité de la relation moment-rotation. Une modélisation analytique a été effectuée dans le but de modéliser le comportement moment-rotation de l'interface fondation-sol. La fondation rigide ainsi que le sol en dessous ont été modélisés par un seul élément qui représente les caractéristiques essentielles du comportement moment-rotation observées dans les essais de centrifugeuse.

1 INTRODUCTION

Soil-foundation interaction associated with heavily loaded shear walls during large seismic events may produce highly nonlinear behavior. Geotechnical components of the foundation are known to have a significant effect on the building response to seismic shaking. The nonlinearity of the soil may act as an energy dissipation mechanism, potentially reducing shaking demands exerted on the building. This nonlinearity, however, may result in permanent deformations that also cause damage to the building.

Six series of tests on a large centrifuge, including 50 models of shallow foundations supporting shear walls, were performed to study the nonlinear load-deformation characteristics of shallow foundations during cyclic and earthquake loading. Footing dimensions, depth of embedment, wall weight, factor of safety, soil density, and soil type (dry sand and saturated clay) were systematically varied. Static vertical loading, slow cyclic horizontal loading at different heights of the wall and dynamic earthquake shaking events were applied to the models to study cyclic and permanent deformation behavior of soil-footing interface at prototype stress levels under typical combinations of moment, shear and axial load.

Analytical modeling was carried out to model the moment-rotation behavior of footing soil interface. The rigid footing and the soil beneath the footing, considered as a single element, was modeled by considering the opening and closing of gaps behind and in front of a contact area that moves based on the geometry of the footing and the shape of the rounded soil-foundation interface. The model captures the essential features of the moment-rotation relationship that were observed in the centrifuge experiments.

2 CENTRIFUGE EXPERIMENTS

Experiments have been conducted in a 9.1m radius centrifuge at the Center of Geotechnical Modeling at the University of California, Davis at 20g centrifuge acceleration. Five series of tests were conducted on dry sand (Dr = 80% and 60%) and one test series was on saturated clay (Cu = 100 kPa). All the models were tested on a soil bed prepared in a rigid container (1.75m x 0.90m x 0.53m, model scale dimensions), each of which included about 8 footing-wall models. All the results in this paper are presented in prototype units unless otherwise stated. The initial static vertical factors of safety of the footings were varied from about 2.0 to 10.0, by changing the weight of the structure and footing dimensions (length (L) = 2.5 m to 4.0 m, width (B) = 0.4 m to 1.0 m, embedment (D) = 0.0 m to 0.7 m). The depth of the soil layer inside the container was 4.0 m.

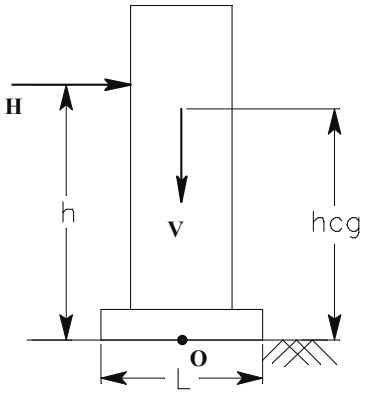

Figure 1 Forces acting on the wall-footing system during slow cyclic lateral push tests

Fig. 1 shows the test setup for slow cyclic lateral load tests that were conducted on structures with different initial static vertical factors of safety (FS_V) (varying footing dimensions, applied vertical load, soil strength) and with height of lateral loading (h) varied (to produce different moment to shear ratio at the base of the footing). Displacements were measured by two horizontal and two vertical linear potentiometers attached on the wall and forces were measured by a load-cell attached to the actuator. Experimental setups, testing procedures and the method of data processing for slow cyclic and dynamic tests are explained in detail in Kutter et al. (2003) and Gajan et al. (2004).

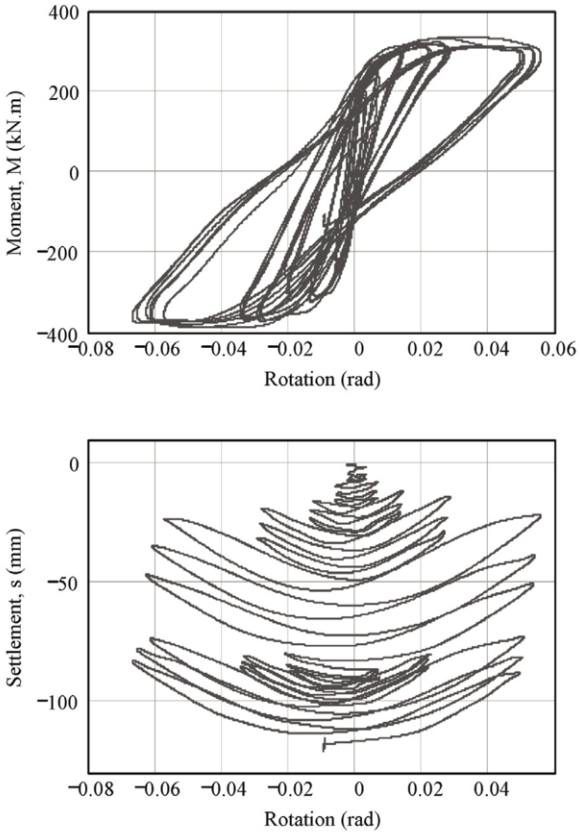

Figure 2 Slow cyclic lateral push test results: dry sand, Dr = 80%, L = 2.84 m, B = 0.65 m, D = 0.0 m, FS_V = 6.7, h = 4.

2.1 *Moment-rotation behavior of footing-soil interface*

Fig. 2 shows the moment-rotation and settlement-rotation relationships at the base center point of the footing for one of the lateral push test (Dr = 80% dry sand, L = 2.84 m, B = 0.65 m, D = 0.0m, h = 4.9 m, and FS_V = 6.7). The moment-rotation relationship encloses a large area in hysteresis loops indicating a considerable amount of energy is dissipated at the footing soil interface. The moment-rotation plot does not show any reduction in moment capacity with the number of cycles or with the amplitude of rotation, but it does show a degradation of rotational stiffness with increasing amplitude of rotation.

The settlement-rotation relationship shows the accumulation of permanent settlement beneath the footing, however the rate of increase in settlement per cycle of rotation decreases with the number of cycles applied. As the footing settles down, its depth of embedment increases, overburden stresses increase, and vertical stiffness also increases, thus the rate of increase of settlement reduces. The settlement-rotation plot shows the uplift behavior of the footing at larger rotation amplitudes. The base of the footing looses its contact with the footing soil when the rotation is large. The formation of a gap on one side of the footing causes yielding of the soil on the other side of the footing, and the yielding of the soil on the other hand increases the uplift. Foundation rocking during high amplitude lateral loading causes rounding of the soil beneath the footing, and the rounding of the soil causes the nonlinear moment rotation relationship and the degradation of rotational stiffness due to closing of the gap.

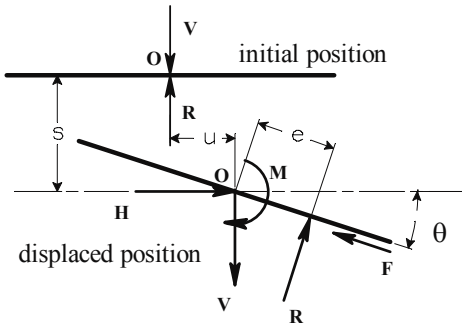

Figure 3 Resultant forces and displacements at the soil-footing interface

2.2 *Rounding of soil beneath footing*

Plaster was cast at the structures' footprint after selected tests to preserve the imprint for subsequent analysis of the shape of the soil surface beneath the footing. Measurements of these footing imprints were taken in transects using a Computer Measuring Machine (CMM). These imprints illustrate the rounding at the foundation soil interface, which cumulated during the slow-cyclic lateral push tests. Rounding of the interface causes partial separation of the footing from the soil, resulting in reduced footing-soil contact area. During moment loading, the footing begins lifting off on either side of its contact, and progressively creates a rounded soil surface beneath the footing. As a result, the length of contact between the footing and soil decreases as the structures' rotation increases and as the rounding of the soil surface becomes significant. The contact length not only reduces, but also moves along the length of the footing as the building rocks, causing a nonlinear bearing pressure distribution in the soil beneath the contact length. The changing location of the resultant of the bearing pressure distribution with the rotation of footing determines the moment-rotation behavior.

3 ANALYTICAL MODELING

3.1 *Forces and displacements at the base of the footing*

Fig. 1 shows a shear wall supported by shallow foundation and the forces acting on it during slow cyclic lateral push tests. Its self-weight, V, acts at the height of center of gravity of the structure (hcg) and a varying lateral load, H, is applied at a height h from the base of the footing. The resultant forces acting on the soil-footing interface are shown in Fig. 3. Initially, the structure is in equilibrium with the opposite and co-linear forces self weight (V) and the soil bearing resistance (R). At displaced position, an over turning moment, M, resulting from both applied lateral load (H.h) and the P-Δ effect when the structure is tilted (V.hcg.sin(θ)), acts at the center of the footing. Because of the interaction between uplift, soil yielding and nonlinear bearing pressure distribution, the resultant bearing force acts at a distance, e, from the base center point (O). The frictional resistance force at the soil-footing interface is indicated by F. Fig. 3 also shows the displacements at the base center point of the footing; settlement (s), lateral displacement (u) and rotation (θ). For the equilibrium of the soil-footing interface, the following relations can be derived.

$$V = R \cdot \cos(\theta) + F \cdot \sin(\theta)$$
$$H = F \cdot \cos(\theta) - R \cdot \sin(\theta)$$

$$M = H \cdot h + V \cdot hcg \cdot \sin(\theta) = R \cdot e \qquad \text{(eq. 1)}$$

At small rotations (for $\theta \le 0.05$ rad.), the above relations can be approximated to,

$$V = R\ ,\ H = F\ ,\ \text{and}\ M = R \cdot e \qquad \text{(eq. 2)}$$

The purpose of this paper is to describe how the moment-rotation and settlement-rotation behavior were modeled analytically and how the coupling between vertical force, bearing pressure distribution and moment was handled. The relationship between horizontal force-sliding, settlement-sliding and the coupling between horizontal force, vertical force and moment are out of scope of this paper.

3.2 *Modeling of moment-rotation behavior*

Analytical modeling was carried out to simulate the moment-rotation behavior of soil-footing interface. Footing and the soil beneath the footing were considered as a single element. As the footing rocks, the soil surface beneath the footing becomes curved as mentioned in the previous section. By keeping track of the shape of the soil surface beneath the footing and the location of the contact area of the footing with soil, the moment-rotation behavior was modeled. The moment-rotation behavior depends on the shape of the bearing pressure distribution and the location of the contact area with the soil surface beneath the footing. The applied external loads cause a change in moment magnitude, which causes the changes in contact location and nonlinear bearing pressure distribution. By equating the moment applied by the external loads to the resisting moment provided by the soil medium (eq. 1), moment-rotation relationship can be obtained.

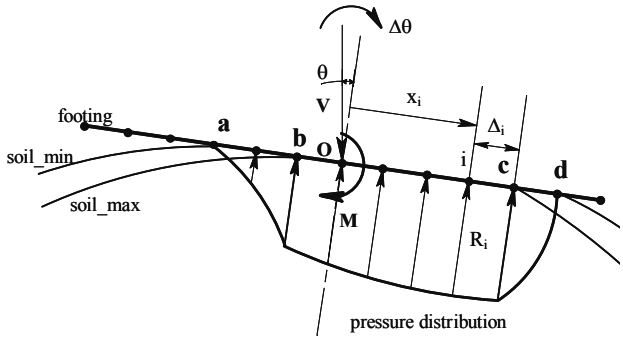

Figure 4. Footing-soil contact element model

Fig. 4 illustrates the concept of the single element contact model. It shows the contact of the footing with the rounded soil surface beneath the footing and the forces acting at the interface. As shown in Fig. 4, soil_min and soil_max represent two different rounded soil surfaces beneath the footing. Soil_max represents the soil surface that contains the maximum settlement experienced by the soil, whereas soil_min represents the surface that exists after the footing leaves the contact with the soil surface as the building rocks. The difference between soil_max and soil_min is attributed to elastic rebound and plastic bulging of soil on the back side of the footing during uplift. The footing is modeled with finite number of nodes, each of which corresponds to a node at soil_min surface and soil_max surface.

3.3 *Contact element method*

For every increment in rotation, the contact length of the footing with the soil, contact points with soil surfaces (soil_min and soil_max), and the bearing pressure distribution along the contact length were updated. Every node has the history of following information that were updated for every loading increment.

1. Location of footing
2. Current soil surface location (soil_min)
3. Maximum past settlement (soil_max)
4. Current bearing pressure
5. Maximum past pressure experienced

Procedure of computation:

1. The incremental rotation ($\Delta\theta$) is applied to the contact element.
2. The point of rotation of the rigid footing, for that $\Delta\theta$, is initially assumed at pint b and the new location of the footing is updated at every node.
3. The shape and the elevation (settlement) of the soil_max surface beneath the footing are updated according to the new position of the footing.
4. The new position of the soil_min surface is located using the rebounding ratio and footing position.
5. The contact nodes of the footing with soil_min and soil_max surfaces at both sides of the footing is found from the new locations of footing and soil surfaces (nodes a, b, c, and d in Fig. 4)
6. The new bearing pressure distribution at every node that is in contact with the soil_max surface (between nodes b and c) is calculated first.

$$R_{i,incr} = R_{i,incr-1} + ds \cdot kv \cdot \left[\frac{L}{Vult}\right] \qquad \text{(eq. 3)}$$

where, $ds = soil\_max_{i,incr} - soil\_max_{i,incr-1}$

In eq. 3, R_i is a dimensionless bearing pressure parameter that indicates the amount of bearing resistance at node i. The vertical stiffness of the soil kv (kN/m^2) is normalized by (Vult/L) to make R dimensionless (Vult is the ultimate vertical load for pure vertical loading and L is the length of the footing). The difference in soil_max layers, ds, includes the total settlement at a node (both elastic and plastic). Elastic part is rebounded when unloaded due to uplift. The pressure between soil_max and soil_min surfaces (between a and b, and c and d) is a parabolic distribution having zero pressures at the extreme contact points (points a and d). The parabolas at the loading side (cd) and unloading side (ab) of the footing have different shapes as shown in Fig. 4. Note that, at every node, R_i should satisfy,

$$0.0 \le R_i \le 1.0 \qquad \text{(eq. 4)}$$

7. The distribution of R along the contact length is integrated to get the total resisting vertical force, say Vr.

$$Vr = \frac{Vult}{L} \cdot \sum_{i=a}^{d} \left[R_i \cdot \Delta_i \cdot \cos(\theta)\right] \qquad \text{(eq. 5)}$$

where, Δ_i is the distance between node i and (i+1)

8. The applied vertical force, Vapp, is compared with the calculated total resistance force Vr. If vertical equilibrium is satisfied within allowable tolerance, the next step proceeds. If not, the procedure goes back to step 2 and adjusts the point of rotation.
9. Finally, the moment is calculated by integrating the product of bearing force distribution and distance along the contact length of the footing.

$$M = \frac{Vult}{L} \cdot \sum_{i=a}^{d} \left[R_i \cdot \Delta_i \cdot x_i \right] \quad \text{(eq. 6)}$$

where, x_i is the distance of node i from footing base center point O.

3.4 *Critical contact length and ultimate moment*

As the magnitude of rotation is increased, the contact length becomes smaller and moves towards the edge of the footing due to uplift at the other side. As the contact length decreases, the bearing resistance intensity along the contact length increases in order to satisfy the vertical equilibrium. At one stage, the bearing resistance along the whole contact length becomes equal to the ultimate bearing resistance; hence, no further reduction in contact length is possible. This minimum contact length is defined as the critical contact length (Lc) and the moment obtained at this stage is the ultimate moment (Mu). Based on this concept, the relations for Lc and Mu are:

$$\frac{Lc}{L} = \frac{1}{FS_V} \quad \text{(eq. 7)}$$

$$Mu = \frac{V.L}{2}\left[1 - \frac{Lc}{L}\right] \quad \text{(eq. 8)}$$

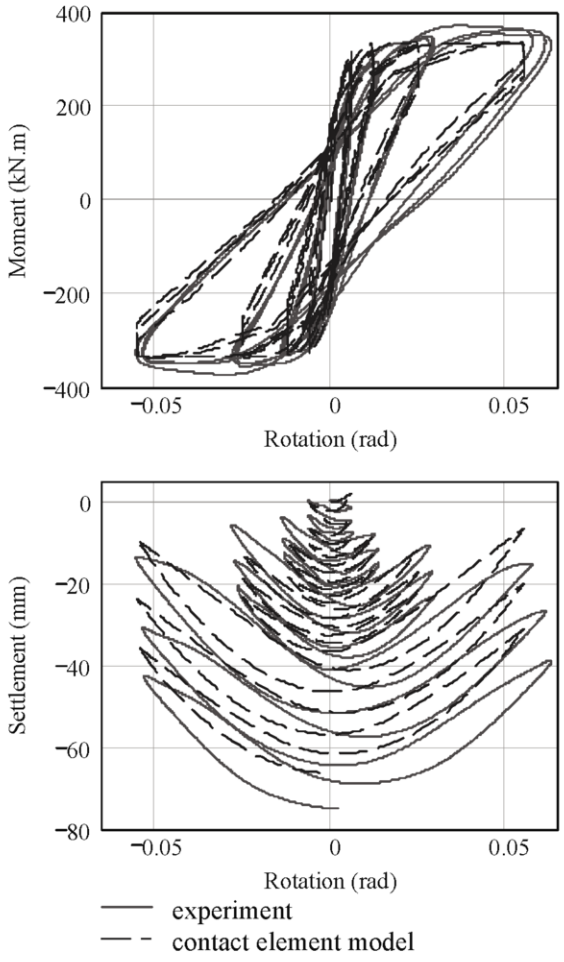

Figure 5 Comparison of contact element simulations with experimental results

4 RESULTS

Fig. 5 shows the results obtained from the contact element model for the structure with L = 2.84 m, B = 0.65 m, D = 0.0 m, h = 4.9 m, and FS_V = 6.7 on dry sand of Dr = 80%. The simulation captures the features observed in moment-rotation-settlement behavior in the experiments. At the beginning, for small rotations, the contact length is closer to L, the curvature of the soil surface is small and the rate of increase in eccentricity with rotation ($de/d\theta$) is large, hence, the moment rotation plot shows higher stiffness. As the rotation goes to higher values, progressive rounding of the soil surface increases the curvature and decreases the contact length. Therefore rotational stiffness degradation is observed at larger magnitudes of rotation. The ultimate moment (Mu) obtained in both experiment and simulation is very close to the theoretical Mu.

The settlement-rotation plot also reproduces the mechanisms observed at the footing soil interface. The dependence of the relationships between settlement-uplift-rotation on the geometry of the soil surface and the contact location of footing is clearly visible in the contact model simulation. Settlement and uplift increase as the magnitude of rotation increases as observed in the experiment. Settlement to rotation ratio ($ds/d\theta$) at various magnitudes of rotations and the permanent settlement from the simulation are close enough to the experimental results. The amount of settlement depends on FS_V, vertical stiffness and the rebounding ratio.

5 DISCUSSION

The analytical contact element model presented in this paper to simulate the moment-rotation and settlement-rotation behavior of rocking shallow foundations makes use of the geometry of the rounded soil surface beneath the footing due to foundation rocking, the changing location of the contact length and the nonlinear bearing pressure distribution along the contact length of the footing. The model is simple, easy to implement and computationally fast. The only three model parameters are: friction angle, vertical stiffness and the rebounding ratio of soil. The model captures the essential features of moment-rotation-settlement relationships observed in the experiments.

ACKNOWLEDGMENTS

This work was supported primarily by the Pacific Earthquake Engineering Research Center's Program of the National Science Foundation under Award Number EEC-9701568 and PEER project number 2262001. The authors would like to acknowledge the suggestions and support provided by Geoff Martin, Tara Hutchinson, Key Rosebrook, Justin Phalen and Dan Wilson.

REFERENCES

Gajan, S., Phalen, J.D., Kutter, B.L., Hutchinson, T.C. and Martin, G.R. Centrifuge Modeling of Nonlinear Cyclic Load-Deformation Behavior of Shallow Foundations. *Proc. of the 11th int. conf. in soil dynamics and earthquake engineering*. University of California, Berkeley. Jan. 2004

Kutter, B.L., Martin, G.R., Hutchinson, T.C., Harden, C., Gajan, S. and Phalen, J.D. Status Report on Study of Modeling of Nonlinear Cyclic Load-Deformation Behavior of Shallow Foundations. *Pacific Earthquake Engineering Research Center's Workshop*. University of California, Davis. March, 2003